

# We are IntechOpen, the world's leading publisher of Open Access books Built by scientists, for scientists

6,900

Open access books available

186,000

International authors and editors

200M

Downloads

Our authors are among the

154

Countries delivered to

TOP 1%

most cited scientists

12.2%

Contributors from top 500 universities



WEB OF SCIENCE™

Selection of our books indexed in the Book Citation Index  
in Web of Science™ Core Collection (BKCI)

Interested in publishing with us?  
Contact [book.department@intechopen.com](mailto:book.department@intechopen.com)

Numbers displayed above are based on latest data collected.  
For more information visit [www.intechopen.com](http://www.intechopen.com)



# Enhanced Fourier Transforms for X-Ray Scattering Applications

Benjamin Poust and Mark Goorsky

*University of California, Los Angeles, Department of Materials Science and Engineering,  
Los Angeles, CA 90095  
USA*

## 1. Introduction

A new method for enhancing the Fourier transforms of x-ray reflectivity data is presented. This enhanced Fourier analysis, which employs differentiation of the scattered intensity signal, is shown to be extremely effective in extracting layer thicknesses from specular x-ray reflectivity scans from single and multi-layer structures. This is a powerful technique that complements simulations of x-ray scattering patterns that employ dynamical diffraction models. Examples of the procedure, data analysis, and comparison of the results with methods that have been described previously will be presented.

A Fourier Transform (FT) power spectrum peak represents the frequency or period length of an interference oscillation. X-ray scattering measurements provide information in the reciprocal space domain. Therefore, the FT of an x-ray scattering measurement would be expected to provide information concerning layer properties, especially the layer thicknesses which establish the interference fringes in scattering measurements including reflectivity measurements and higher angle diffraction measurements. Indeed, the intensity modulations that are observed in specular x-ray reflectivity measurements are related to the layer thicknesses and to the difference in refractive index between one layer and the next. At x-ray wavelengths, the refractive index is determined by the material density. Discrete Fourier transforms and their application to x-ray reflectivity data will be discussed subsequently in terms of the mathematics, challenges inherent to x-ray scatter FTs, and enhancement techniques that have already been discussed in the literature.

The key to the enhancement method described here is based around **differentiating** the specular intensity with respect to vertical reciprocal space coordinate  $Q_z$ . This differentiation retains the important and useful components of the x-ray reflectivity measurements while minimizing the impact of features of the measurements that obscure the transformation of the interference pattern. The reflectivity data is transformed according to

$$I_j^T = \frac{dI_j}{dQ_{z,j}} \approx \frac{1}{N} \sum_{i=1}^N \frac{I(Q_{z,j+i}) - I(Q_{z,j-i})}{Q_{z,j+i} - Q_{z,j-i}} \quad (1)$$

The summation on the right side of the equation is over the  $N$  nearest data points on either side of the  $j^{\text{th}}$  data point. The number of neighboring data points used to calculate the

average slope at the  $j^{\text{th}}$  data point is set just high enough to average out noise fluctuations, but kept well below the period lengths of any possible thickness signals. In general, this differentiation approach is far more effective at removing the sloping background than logarithmic compression alone, average subtraction alone, or  $Q_z^4$  leveling (Durand's method (Durand 2004)) methods in the literature which have been previously employed to enhance FT of the reflectivity data and these methods are described in more detail below. When combined with any of the other enhancement techniques, however, differentiation yields readily distinguishable FT peaks for even the weakest and most truncated of sloping oscillations. It is not proposed here that differentiation should replace the other enhancement techniques, but rather that it should be used with them to achieve the best possible FT enhancement. The background into the development of this approach is presented below with illustrations and comparison with the other techniques.

## 2. Background

Electromagnetic radiation that travels through one medium and passes into another will be partially reflected at that interface if the media have different indices of refraction. Radiation reflecting from interfaces leads to interference in the scattered wave and it is this effect that makes x-ray scatter based film thickness measurements useful. X-ray reflectivity can be especially amenable to extraction of layer thicknesses as the interference pattern includes only information on changes in refractive index (which is the electron density at x-ray wavelengths) as a function of depth. The crystallinity, strain state, or other such crystallographic factors do not play roles in determining the reflectivity curve for both substrates and multi-layer structures deposited on the substrates. In fact, specular x-ray reflectivity measurements have proven to be extremely valuable for determining the properties of multi-layer structures. In a typical case, the fringes that are introduced from a single layer are used to determine the layer thickness; for more complicated multi-layer structures, simulation programs are used to help extract layer thicknesses.

To demonstrate the information gained from a specular x-ray reflectivity scan, consider that the reflectivity scan is simply a specular scan from the origin (000) of reciprocal space along  $Q_z$ , i.e., perpendicular to the surface. This is depicted in Figure 1 which shows a two dimensional section of reciprocal space that includes the co-planar scattering conditions; the so-called Ewald construction. An 'off-specular' scan, which will be described later as an important scan used in the literature to help extract thickness information via FT, is also included in the figure.

The axes are  $Q_x$ , which is along the surface, and  $Q_z$ , which is perpendicular to the surface.  $K_o$  represents the incident wavevector (with a magnitude  $1/\lambda$  where  $\lambda$  is the radiation wavelength) and  $K_H$  represents the scattered wavevector (also  $1/\lambda$ ). For specular reflectivity scans, the angle between the incident beam and the surface is  $\omega$  ( $= \Theta$ ) and the angle between the incident and scattered beams is  $2\Theta$ . Changing  $\omega$  ( $=\Theta$ ) by a small increment and the angle between the incident and scattered beams by twice that increment traces a vertical line in reciprocal space. The relationship between  $Q_z$  and  $\omega$  and  $2\Theta$  is simply

$$Q_z = \frac{(\sin \omega - \sin(\omega - 2\Theta))}{\lambda} \quad (2)$$

and, for the specific case for specular reflectivity where  $\omega = \Theta$ ,

$$Q_z = \frac{2(\sin \Theta)}{\lambda} \quad (3)$$

It should be noted that, at x-ray wavelengths, the refractive index is important. Including this effect leads to

$$Q_z = \frac{2}{\lambda} \sqrt{\cos^2 \Theta_c - \cos^2 \Theta} \quad (4)$$

where  $\cos(\Theta_c)$  = the refractive index and  $\Theta_c$  represents the critical angle below which the incident x-ray beam is totally reflected at the surface. (Durand 2004)

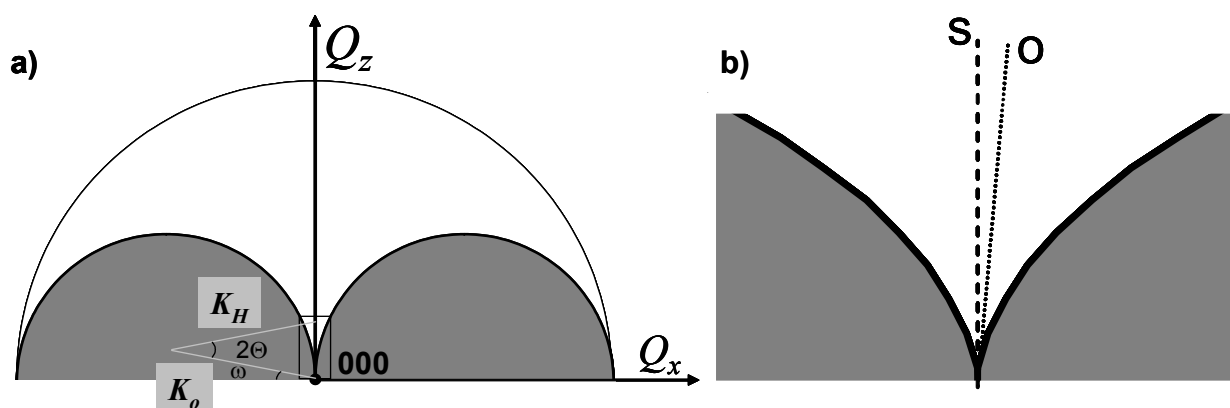


Fig. 1. Reciprocal Space and the Ewald Construction. (a) The two gray half circles represent regions for which scattering involves the transmission mode. The region near the origin of reciprocal space (000) is expanded in (b). The vertical dashed line (labeled 'S') represents a specular reflectivity scan. This is achieved by rotating the sample by an angle  $\omega = \Theta$  with respect to the incident beam and the angle between the incident and scattered beam by  $2\Theta$ . The dotted line (labeled 'O') represents an off-specular scan in which the incident beam angle with the surface  $\omega \neq \Theta$  but both the angle  $\omega$  and  $2\Theta$  are moved by increments of  $\Theta$  and  $2\Theta$ , respectively

The development of x-ray reflectivity expanded significantly with the work of L.G. Parratt (Parratt 1954), who introduced a theory that related the layer thicknesses and electron densities to the reflectivity curve. Following the approach of von Laue, Parratt used Maxwell's equations and appropriate boundary conditions to solve for the reflected to transmitted amplitude ratio at the bottom of layer  $j$ ,  $X_j$ :

$$X_j = \frac{r_j + X_{j+1}\varphi_{j+1}^2}{1 + r_j X_{j+1}\varphi_{j+1}^2} \quad (5)$$

where layer  $j + 1$  is below layer  $j$ . The phase offset of the wave scattered from the bottom of and traversing the thickness of layer  $j + 1$ ,  $\varphi_{j+1}$ , is:

$$\varphi_{j+1} = \exp(ik_{z,j+1}t_{j+1}) \quad (6)$$

The component of the wave vector perpendicular to the surface in layer  $j$ ,  $k_{z,j}$ , is

$$k_{z,j} = \frac{1}{\lambda \sqrt{n_j^2 - \cos^2 \Theta}} \quad (7)$$

where  $\omega$  ( $= \Theta$ ) is the incidence angle, as noted above, and  $n_j$  is the index of refraction of layer  $j$  at wavelength  $\lambda$ .

The Fresnel coefficient of reflection from the interface between layers  $j$  and  $j + 1$ ,  $r_j$ , is given by

$$r_j = \frac{k_{z,j} - k_{z,j+1}}{k_{z,j} + k_{z,j+1}} \quad (8)$$

for a sharp interface.

Overall, the x-ray reflectivity  $R(Q_z)$  for a layer on a substrate can be described as

$$R(q_z) = \frac{I(Q_z)}{I_o} = R_F(Q_z) \left| \frac{1}{\rho_\infty} \int \frac{d\rho(z)}{dz} \exp(iQ_z z) dz \right|^2 \quad (9)$$

where  $I_o$  is the incident intensity,  $I(Q_z)$  is the measured reflectivity intensity, and  $R_F(Q_z)$  is the Fresnel reflectivity (which is effectively the Fresnel coefficient [8] squared). Equation [9] demonstrates that the reflectivity intensity as a function of  $Q_z$  (or  $\Theta$ ) depends only upon the density change at the interfaces and surface.

This relationship later modified the Fresnel coefficient to account for rough or graded interfaces:

$$r_j = \frac{k_{z,j} - k_{z,j+1}}{k_{z,j} + k_{z,j+1}} \exp\left[-2\sigma_{j+1} \sqrt{k_{z,j} k_{z,j+1}}\right] \quad (10)$$

where  $\sigma_{j+1}$  is the effective width associated with interface roughness and/or compositional grading. Further development of the theory of x-ray reflectivity scattering is addressed elsewhere. (Bowen and Tanner 1998; Daillant and Gibaud 1999; Wormington, Panaccione et al. 1999)

Examples of reflectivity curves based on this formalism are shown below to illustrate the application and challenges associated with using Fourier Transforms of x-ray reflectivity data to extract layer thickness information. Figure 2 shows reflectivity from a silicon surface, a silicon surface with a layer of SiO<sub>2</sub>, a silicon surface with a layer of germanium, and a silicon surface with an r.m.s. roughness of 5 Å.

For such specular reflectivity scans, it is customary to plot the intensity on a logarithmic scale against the angle  $\omega$  (which, for a specular scan is equal to  $\Theta$ ) with the understanding that the angle between the incident beam and the detector is also changing at twice the angle, hence  $2\Theta$ . In some cases, the x-axis will indicate this, e.g., with a label ' $\omega - 2\Theta$ ' or ' $\Theta - 2\Theta$ '. In other cases, the reflectivity scan will be plotted as a function of  $Q_z$  (transformed using equation [2] or [4]).

Starting with the simulated reflectivity curve from a smooth silicon surface, there are two notable characteristics of the specular reflectivity scans that are important for the subsequent Fourier transform:

- i. the reflected intensity is unity when the incident angle is below a certain value – the critical angle for total external reflection which is identified as  $Q_{z,c}$  or  $\Theta_c$  as noted above.

- ii. the reflected intensity drops off strongly for  $Q \geq Q_{z,c}$  ( $\omega \geq \Theta_c$ ) with a with a  $Q_z^4$  dependence at higher angles.

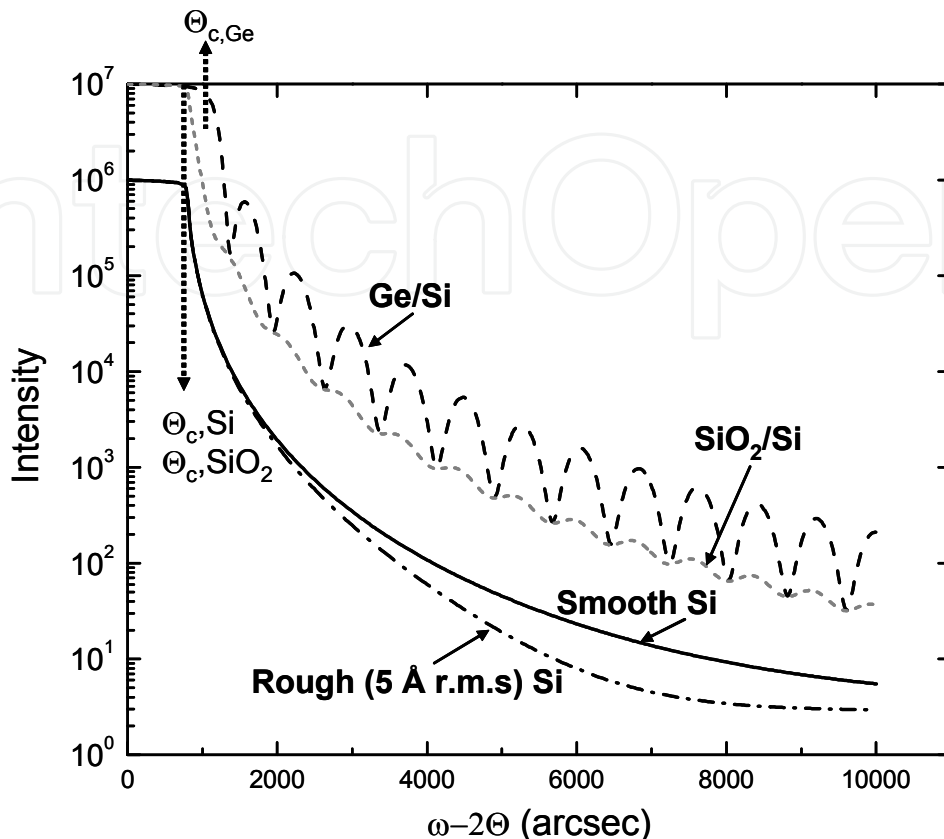


Fig. 2. Simulated X-ray reflectivity scans for a bare surface (Si) comparing \smooth and rough surfaces as well as the scans for 200 Å layers (either SiO<sub>2</sub> or Ge) on smooth Si in which the thickness fringes are clearly visible. The scans from the structures with the SiO<sub>2</sub> and Ge layers are vertically offset (10X) for clarity

For the case of a layer deposited on the silicon surface, a series of fringes is observed. The fringe spacing provides information on the layer thickness and represents interference associated with the difference in electron density between the layer and the substrate. This effect is clearly depicted for the examples of a 200 Å germanium layer on the silicon when compared to a 200 Å layer of SiO<sub>2</sub> layer on silicon. The difference in electron density between silicon and germanium is significantly greater than that between SiO<sub>2</sub> and silicon. The fringe spacing remains the same, whereas the fringe amplitude is correspondingly greater for the combination with the greater electron density difference, in this case, for the germanium on silicon. In addition, the critical angle,  $\Theta_c$  for the Ge layer on the surface is greater than that for the SiO<sub>2</sub> layer on the surface. Silicon and SiO<sub>2</sub> have very similar densities, so the critical angles for those surfaces are also nearly the same value, as shown in the figure.

For the silicon surface with the rougher interface, the intensity drops off at a different  $Q$  dependence (and this decay depends on the extent of roughness). Figure 3 plots the silicon reflectivity multiplied by  $Q_z^4$  ( $\omega^4$  for these scans to compare directly to the data in Figure 2) for the specular scans from both the smooth and the rough surfaces. In these case, it is clear that a horizontal line is generated for the smooth surface for  $\omega > 3\Theta_c$  (i.e., the decay exhibits a  $Q_z^{-4}$  dependence) and a decreasing slope is observed for the rougher surface.

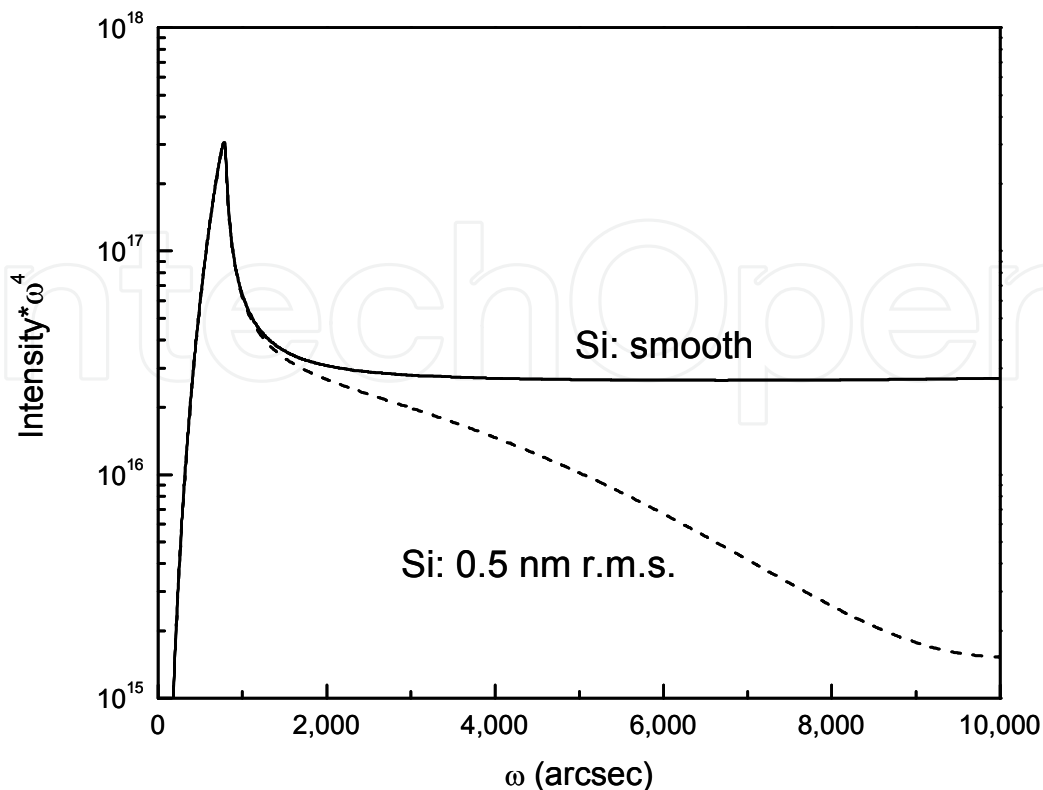


Fig. 3. The intensity at each position is multiplied by the incident angle to the fourth power. For a smooth surface, this product is a constant value at higher angles. For a rough surface, the product decreases at higher angles, but not as strongly as the intensity alone decreases

Based on the x-ray reflectivity curves and as is deduced from Equation [9], x-ray reflectivity scans along  $Q_z$  measure the Fourier transform of the derivative of the electron density with respect to  $z$ . Indeed, Equation [9] can be rewritten as (Russel 1990) (Li, Muller et al. 1996) (Daillant and Gibaud 1999) (Durand 2004)

$$I(Q_z) \approx \frac{1}{Q_z^4} \left[ F\left(\frac{d\rho(z)}{dz}\right) \right]^2 \approx \frac{1}{Q_z^4} P\left(\frac{d\rho(z)}{dz}\right) \quad (10)$$

where, in this case,  $F(d\rho(z)/dz)$  is the Fourier Transform amplitude, and  $P(d\rho(z)/dz)$  is the Fourier transform power of the derivative electron density at a depth  $z$  from the surface. This formulation of the equation more clearly brings out the general  $Q_z^4$  dependence and also suggests that the extraction of the density distribution as a function of depth using Fourier Transforms should be straightforward.

In other words, the Fourier transform of a specular reflectivity measurement should yield the autocorrelation function of the derivative of the electron density. Thus, x-ray reflectivity Fourier transforms are expected to produce peaks corresponding to distances between interfaces, which can be the thickness of individual layers or the sum of the thicknesses of multiple layers, etc. While the order of the interface stack sequence and information about roughness are not extracted directly from a Fourier Transform of the data, the FT extraction is nonetheless anticipated to be powerful techniques for automatically extracting layer thickness from specular reflectivity measurements.

### 3. Experimental background

A Bede Scientific, Inc. model D1 high resolution x-ray diffractometer was used for all x-ray measurements in this work. The diffractometer is comprised of three primary components, often referred to as 'axes.' The first 'axis' is the beam conditioning component of the diffractometer, the second is the sample alignment and the third includes the scattered beam conditioning.

The first axis collimates and monochromates the x-ray radiation produced using a copper anode ( $\lambda_{\text{CuK}\alpha 1} = 1.540562 \text{ \AA}$ ) vacuum tube x-ray. A Maxflux<sup>TM</sup> specular mirror is used to redirect divergent x-rays toward the collimator crystal in a parallel path, resulting in an approximately tenfold increase in usable x-rays. In the reflectivity measurements discussed here, the beam is diffracted twice by one channel-cut 220 Si collimator crystal and then passed through a slit before it is incident upon the sample crystal. Together, the specular mirror, collimator crystal, and monochromator slit comprise the first axis.

The second axis supports and manipulates the sample crystal, or specimen. The specimen can also be rotated along orthogonal axes in the plane of the sample surface:  $\chi$  and  $\omega$ . The  $\chi$  axis of rotation allows for adjustment of sample tilt and is located in the dispersion plane of the diffractometer.  $\omega$  is orthogonal to  $\chi$  and describes the angle of incidence between the x-ray beam and the sample surface, as noted above.

The third axis assembly is placed on a cantilever that revolves around the  $2\theta$  axis of rotation, which coincides with the  $\omega$  axis of rotation. A scintillating x-ray detector tuned for optimum response to the copper K $\alpha$  line, a dual-channel analyzer crystal (DCA) ((220) silicon reflections), and a pair of x-ray acceptance limiting detector slits constitutes the scattered beam conditioning axis. The configuration of the third axis determines the angular resolution of the instrument. Angular resolution is determined by the width of the detector slits used in double axis measurements which are employed here. In triple axis measurements, the DCA essentially serves as an extremely narrow detector slit and determines the angular resolution of the measurement.

A commercial simulation program (Bede REFS) employs a distorted wave Born approximation to the dynamical scattering conditions. Following the general approach described by Parratt, (Parratt 1954) (Wormington, Panaccione et al. 1999), this program can be used to generate scans for illustrative purposes as well as to help understand the Fourier transforms from multi-layer structures. The examples that are illustrated here employ two different sets of samples. The first includes a thin AlN layer deposited on a sapphire substrate. The second is a multi-layer structure based on an AlSb / InAs structure deposited on a GaAs substrate. The techniques and procedures described here, however, are not material dependent and the structures should be considered as illustrating the general principles of the technique.

### 4. Prior studies: Fourier Transform of specular x-ray reflectivity

The first published use of FT with x-ray scattering data is that of Sakurai and Iida. (Sakurai and Iida 1992) As it happens, a few properties of x-ray reflectivity data that are shown in Figures 2 and 3 severely limit the effectiveness of Fourier transforms of the raw data. Consider that thickness fringes in reflectivity measurements typically follow an intensity distribution illustrated by the curve of the Ge (or SiO<sub>2</sub>) layer on silicon (as in Figure 2); this presents a challenge in that the oscillations appear on a sloping background that ranges over

several orders of magnitude. In the case of a specular x-ray reflectivity scan, the intense peak adjacent to the oscillations is the intense highly reflected component near the critical angle,  $\theta_c$ . The part of the curve containing the oscillations represents a short non-background interval. Any short non-background interval is essentially a signal consisting of a single pulse. A non-square pulse yields a Fourier transform with a truncation peak centered at zero frequency similar to the squared sinc function associated with a square pulse FT. When the oscillations are weak or the number of oscillations measured is small, the truncation peak can obscure the oscillation peaks. This effect is illustrated in Figure 4. Here, a simple sinusoidal oscillation is compared to the same sinusoidal oscillation with the addition of an intense peak at the left that corresponds to the overall decay of the reflectivity signal.

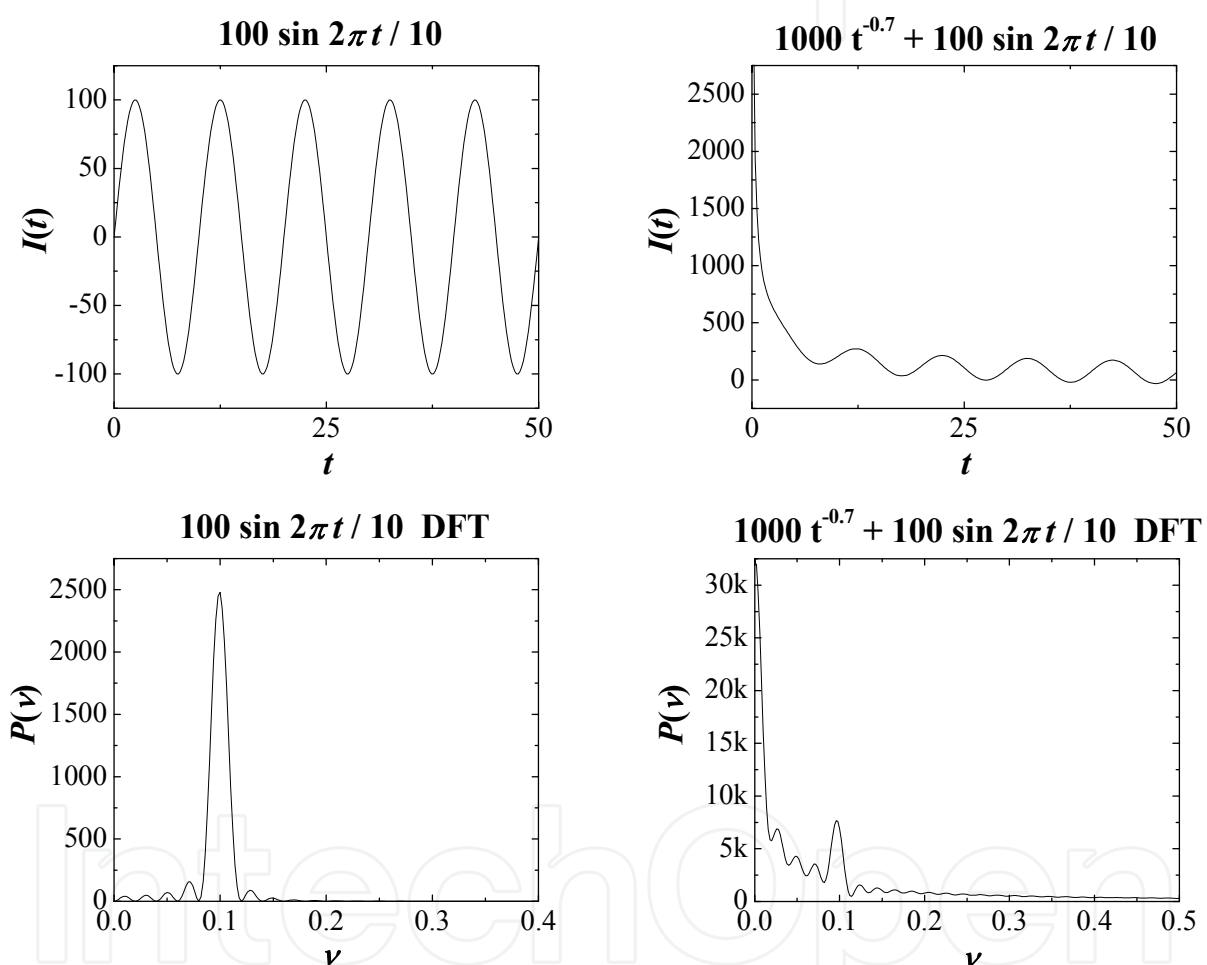


Fig. 4. A sinusoidal oscillation (left, upper) and FT (left, lower), the same oscillation added to half of an adjacent intense peak (right, upper) with the FT showing the peak due to the sinusoidal oscillation partially buried by the truncation FT peak

The FT that includes the high intensity signal at low angles superimposes a truncation FT that significantly distorts the peak which originates from the sinusoidal function. Therefore, the FT provides only vague information about the sinusoidal function peak. This effect is often so severe for experimental data that it renders Fourier transforms on raw data totally useless. For example, see Figure 5. The specular x-ray reflectivity data is from a 320 Å AlN layer deposited on a sapphire substrate and the expected AlN thickness fringe pattern is clearly exhibited. The transform shown on the right, however, only exhibits a diffuse

feature where a sharp peak associated with the 320 Å AlN film would be expected. Clearly, the FT of this data does not provide practical information about the layer thickness and the culprit is the high intensity at low angles that introduces the background slope.

In large part, these types of constraints have limited the popularity of FT analysis with x-ray scatter data. However, a few approaches for enhancing specular x-ray reflectivity FTs exist in the literature. They are based around (i) flattening the overall shape of the x-ray scatter data prior to the FT and (ii) maintaining as much of the interference pattern as possible without artificially modifying the data.

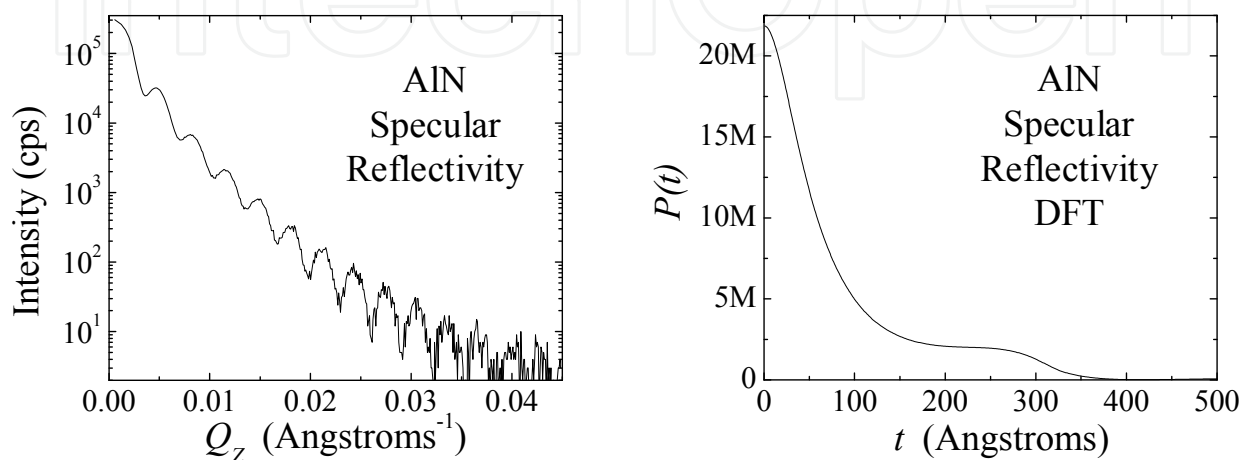


Fig. 5. (Left) X-ray reflectivity scan from a 320 Å AlN film on a sapphire substrate and (right) Discrete Fourier Transform

For example, Banerjee et al., (Banerjee, Raghavan et al. 1999) attempted to flatten the scatter data by subtracting an off-specular scan from the specular reflectivity scan, as is depicted in Figure 1(b). The second technique proposed by Grave de Peralta and Temkin (Peralta and Temkin 2003) involves logarithmic compression of the intensity and subtraction of a heavily smoothed version of the x-ray reflectivity curve. The third technique proposed by Durand (Durand 2004) involved multiplication of the intensity by the reciprocal space coordinate value,  $Q_z^4$  as was already shown in Figure 3. The analysis of each of these concepts is included below.

Because off-specular scans diverge from the interference direction, they often do not show interference fringes. They do, however, have a sloping background shape similar to that of a specular scan. The idea of leveling the specular reflectivity scan for FT enhancement was first demonstrated through subtraction of an off-specular scan for just this reason. (Banerjee, Raghavan et al. 1999) However, the effectiveness of off-specular scan subtraction depends heavily upon the sample measured. A film that is uniform in thickness but conforms to a rough substrate, for example, may have the interference fringes broadened horizontally in reciprocal space. This is because areas of different surface height may scatter incoherently with respect to one another. Such broadened interference fringes are typically referred to as Bragg sheets. They are illustrated in Figure 6.

This effect is demonstrated in Figure 7 which shows the specular scan from the 200 Å Ge layer on Si but with 5 Å roughness at both the Si-Ge interface and the Ge surface. In the latter case, subtraction of the fringes in the off-specular (otherwise known as a longitudinal scan) case will introduce an additional, artificial modulation.

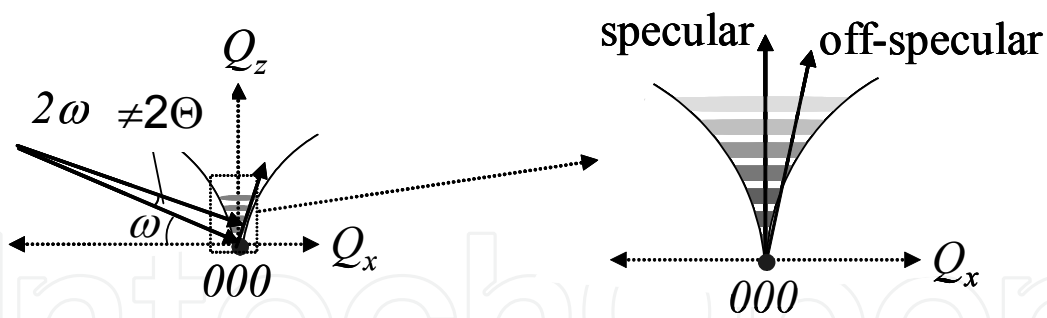


Fig. 6. Specular and off-specular scans in the case where interference fringes are horizontally broadened into Bragg sheets

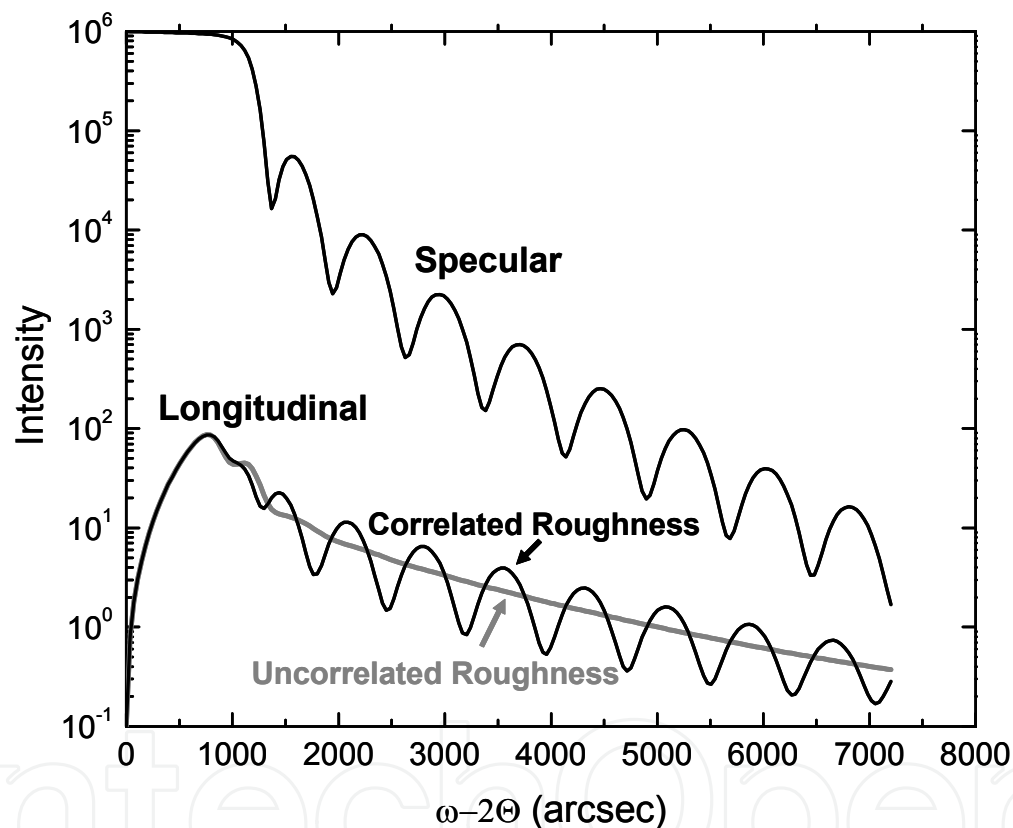


Fig. 7. X-ray reflectivity scans from a 200 Å Ge layer on Si with 5 Å roughness at the interface and 5 Å roughness at the Ge surface. The top scan is the specular scan; the lower scans represent the longitudinal scans for the cases of uncorrelated and correlated interfaces. Still, the use of the off-specular subtraction introduced the idea of leveling the scan by some type of subtraction to enhance the FTs and thus paved the way for more effective techniques.

One improvement is logarithmic compression of the experimental data followed by subtraction of a semi-local average intensity. (Peralta and Temkin 2003) Here logarithmic compression means transforming the intensity of the  $j^{\text{th}}$  datapoint,  $I_j$ , according to:

$$I_j^T = \log I_j \quad (11)$$

Equation [11] transforms the data such that its shape becomes numerically what it appears to be when plotted on a logarithmic intensity scale. When logarithmic compression is first applied, and the semi-local average is then calculated and subtracted, a dramatic reduction of the pulse transform peak is observed upon the Fourier Transform and the oscillation peak is clearly observed, as shown in Figure 8 for the same AlN on sapphire sample discussed earlier. The combination of logarithmic compression and average subtraction is effective because logarithmic compression aids in calculation of a more useful average curve. In this work, the local average is calculated at the  $j^{\text{th}}$  data point as the average over the  $N$  nearest data points in each direction. The average at each point is referred to here as a  $2N$  point local average, where  $2N$  is the number of neighboring points contributing to the average. Within  $N$  data points of each edge of the scan, the number of points used to calculate the average must be reduced. For example, at the first data point (e.g.  $j = 1$ ) the average can only be calculated over data points 1 to  $1 + N$ . Logarithmic compression prior to calculation of the average reduces this effect through simple compression of the intensity dynamic range.

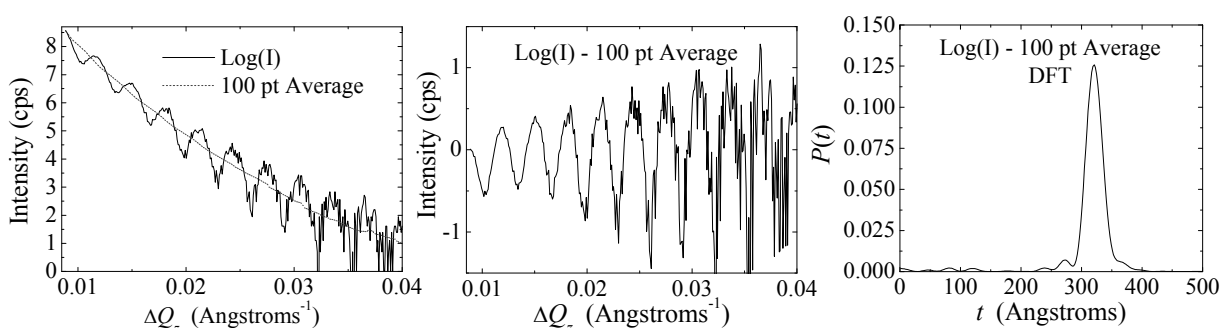


Fig. 8. (Left) logarithmically compressed specular scan showing 100 point local average, (center) specular scatter intensity following subtraction of 100 point local average, and (right) FT of the center curve

Clearly logarithmic compression followed by subtraction of a semi-local average can be very useful. When extremely thin films are measured, however, the approach loses its effectiveness because the wavelength of the oscillation begins to approach the total length of the scan. To prevent the average from itself including oscillations, the term  $N$  must be larger than a period length. When that period length is long,  $N$  must be so large that the average curve no longer matches the sloping background shape. This particular effect is demonstrated in Figure 9 using part of the AlN on sapphire scan. Under these conditions, two extra peaks are artificially introduced into the FT and two thinner layers would appear to be present in the original data.

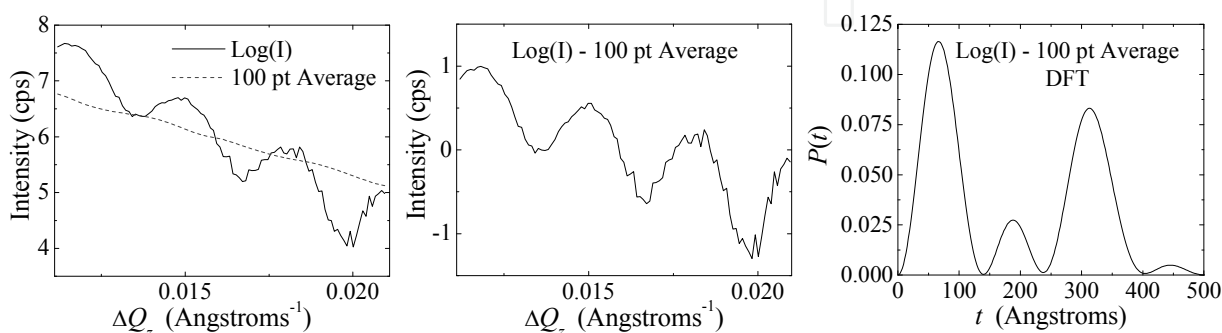


Fig. 9. Log compression and average subtraction with FT for a sample with few fringes

Additional challenges arise when intense peaks exist in the specular scan. This occurs, for example, in the case of a superlattice structure. The peak elevates the average curve above the background slope and thus limits the effectiveness of average subtraction in leveling the data. Improper leveling leads to pulse transform artifacts similar to those observed in Figure 9.

Multiplication of the intensity by  $Q_z^4$  (or  $\omega^4$ ) (Durand 2004) should thus be an effective method for removing the sloping background of a reflectivity scan, i.e., leveling the curve, as depicted in Figure 3. The FT of the leveled curve is calculated and peaks are taken to represent layer thicknesses and sums of layer thicknesses. The effectiveness of this approach is demonstrated using the AIN on sapphire reflectivity data and is shown below in Figure 10.

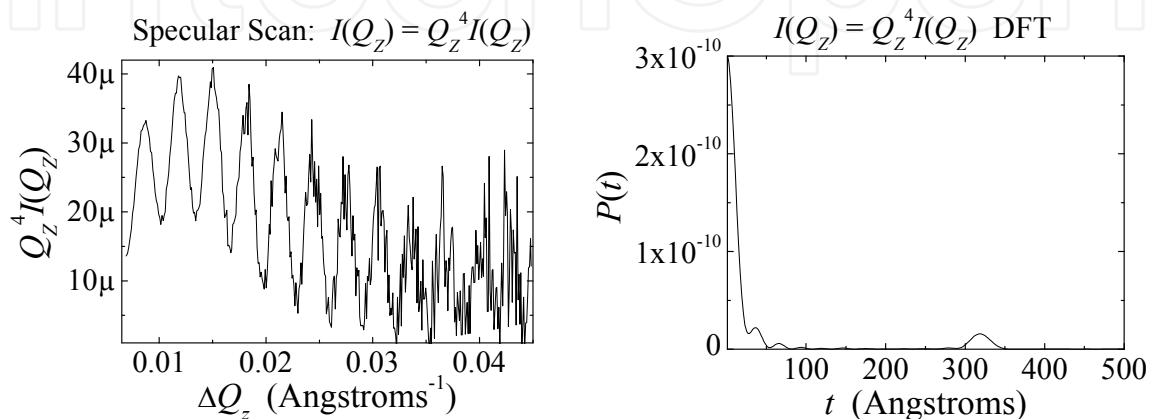


Fig. 10. Multiplication of intensity by  $Q_z^4$  at each data point and the FT showing a distinct peak corresponding to the 320 Å thickness of the layer

As seen in Figure 10, this approach is clearly less effective at leveling the specular scan than are the averaging techniques and thus yields a stronger pulse transform peak. Challenges arise when roughness or graded interfaces cause the specular scatter intensity to drop-off faster with increasing  $Q_z$  (for example, see Figure 2) than the assumed fourth order dependence so the resulting curve is not necessarily flat. The main advantage to Durand's approach, however, lies in the fact that it is independent of oscillation period length. Recall that when subtracting a semi-local average, the optimum local average size must be selected very carefully. Furthermore, when the oscillation period length approaches the length of the measurement, the average subtraction technique becomes ineffective. These disadvantages do not apply to Durand's method. Each of the above techniques has merits, but each suffers from some aspect of the nature of the x-ray reflectivity curve.

## 5. Presentation of a new enhancement approach

### 5.1 Differentiation and application to a single layer structure

An approach to better flatten the reflectivity data stems from considering that the x-ray reflectivity data effectively consists of a well-behaved fringe pattern (sine curves or the combination of several sine curves) with the addition of a sloped background (i.e., the  $Q_z^4$  decay with  $Q_z$ ). These extrinsic influences may be better separated using differentiation than the techniques described in the literature and this concept forms the basis for the approach described here. For example, the differentiation of the fringe pattern will produce a curve with an identical periodicity as the original data while the differentiation of the sloping component will provide a much reduced contribution to the entire curve. The data is transformed according to

$$I_j^T = \frac{dI_j}{dQ_{z,j}} \approx \frac{1}{N} \sum_{i=1}^N \frac{I(Q_{z,j+i}) - I(Q_{z,j-i})}{Q_{z,j+i} - Q_{z,j-i}} \quad (12)$$

The summation on the right side of equation [12] is over the  $N$  nearest data points on either side of the  $j^{\text{th}}$  data point. The number of neighboring data points used to calculate the average slope at the  $j^{\text{th}}$  data point is set just high enough to average out noise fluctuations, but kept well below the period lengths of any possible thickness signals.

Differentiation alone is extremely effective at leveling the data for FT enhancement. As a comparison to logarithmic compression, semi-local average subtraction, and multiplication of the intensity by  $Q_z^4$ , the same specular reflectivity scan of an approximately 320 Å AlN film deposited on a sapphire substrate is shown following the differentiation transformation according to Equation [12] with the FT in Figure 11. The surface truncation peak is significantly reduced and does not overlap with the FT peak due to the layer. Also, the layer peak is relatively sharp and provides the correct layer thickness of 320 Å. Thus, for this example, differentiation is clearly one of the most effective single enhancement techniques. Multiple differentiation processes improve the result further.

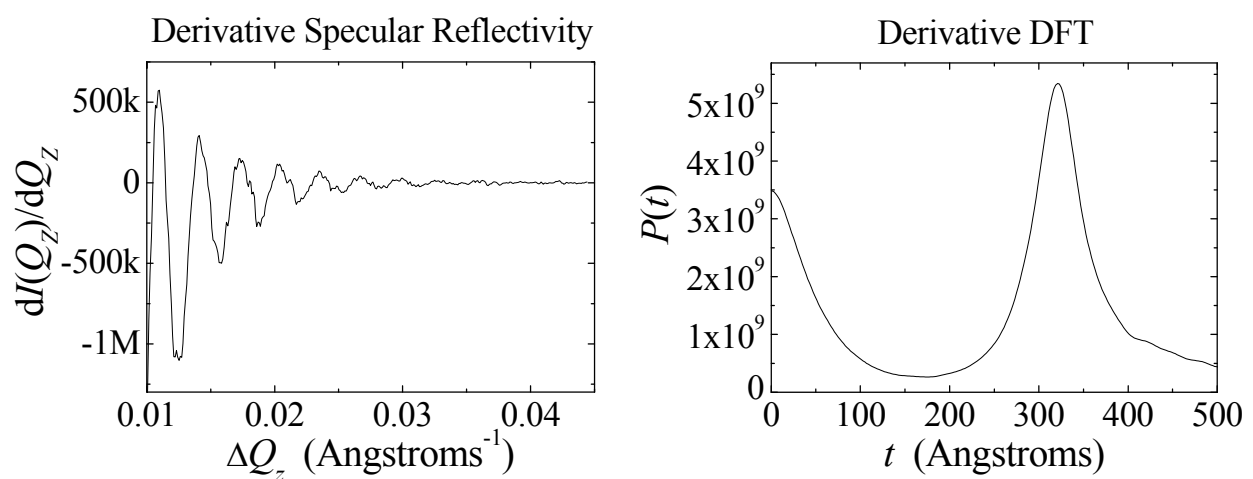


Fig. 11. 320 Å AlN film on sapphire derivative specular reflectivity scan and the FT

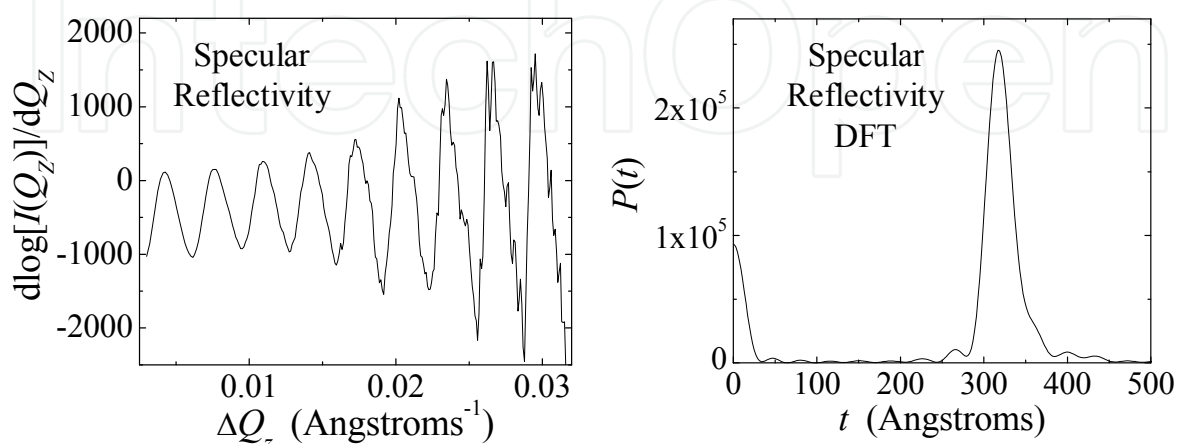


Fig. 12. Specular reflectivity scan with logarithmic compression followed by differentiation (left) and the FT (right)

In general, differentiation is far more effective at removing the sloping background than logarithmic compression alone, average subtraction alone, or the  $Q_z^4$  leveling methods. However, these techniques can be combined to produce even better results. For example, when combined with any of the other enhancement techniques, differentiation yields distinguishable FT peaks for even the weakest and most truncated of sloping oscillations. Therefore, it is not proposed here that differentiation should replace the other enhancement techniques, but rather that it should be used synergistically with one or more of them to achieve the best possible FT enhancement. To illustrate this point, as shown in Figure 12, logarithmic compression followed by differentiation is a very effective transform for FT enhancement of specular reflectivity scans. The peak near 320 Å corresponding to the thickness of the AlN film is clearly observed in the FT and the layer FT peak is sharper than with either technique alone.

Multiplication by  $Q_z^4$  followed by differentiation is also an extremely effective enhancement for specular reflectivity FTs. Using data from the same AlN thin film discussed in the examples above, the FT result is improved through multiplication of the intensity by  $Q_z^4$  followed by differentiation. The curve and FT are shown below in Figure 13.

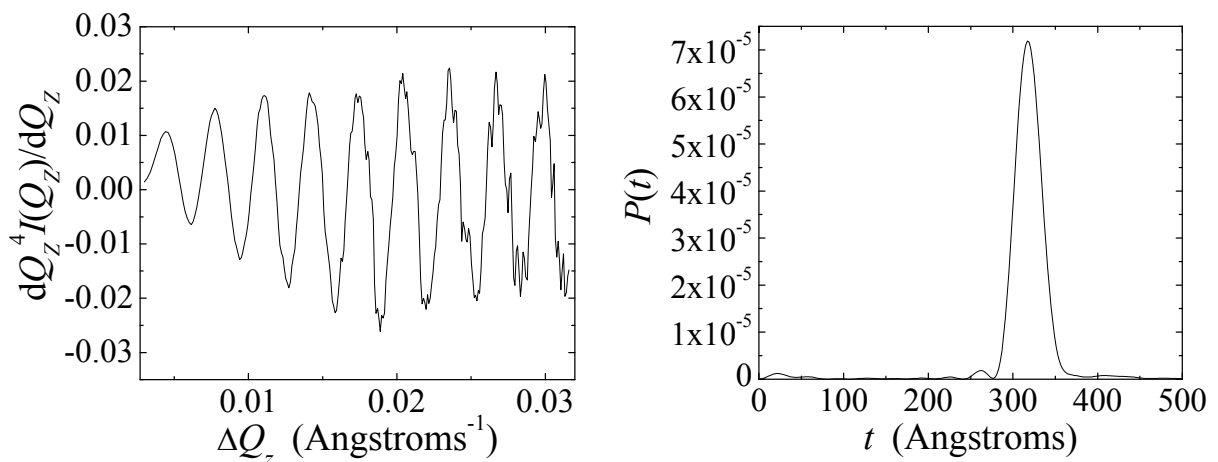


Fig. 13. 320 Å AlN specular x-ray reflectivity curve leveled using  $Q_z^4$  leveling followed by differentiation (left) with the FT (right)

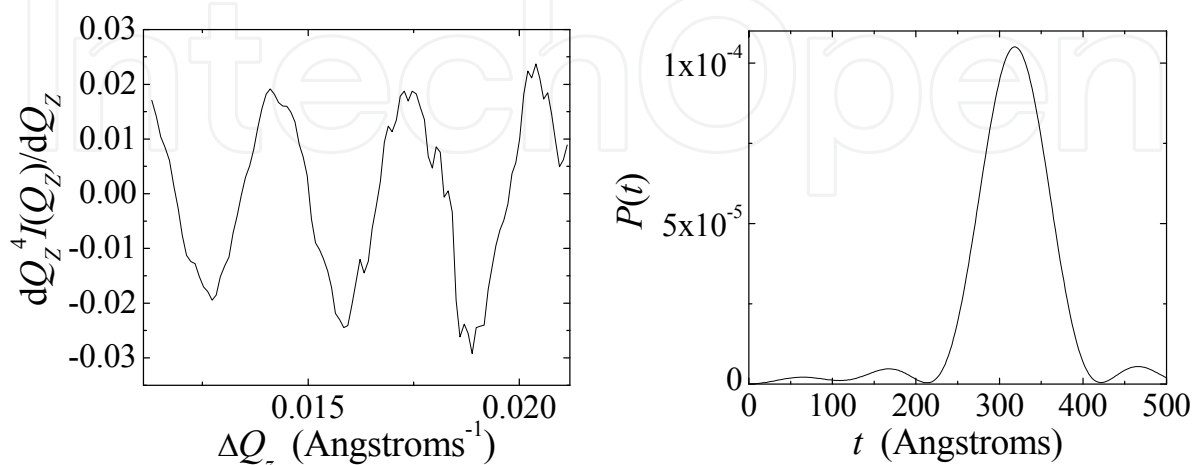


Fig. 14. Truncated 320 Å AlN specular x-ray reflectivity curve leveled using  $Q_z^4$  leveling followed by differentiation (left) with the FT (right)

For comparison to logarithmic compression followed by local average subtraction, the same truncated segment of the AlN reflectivity scan (compare to Figure 9) is processed using  $Q_z^4$  leveling followed by differentiation in Figure 14. Despite the severe wave truncation, the enhanced FT still shows an easily distinguishable single layer thickness peak and greatly reduced artifacts when compared to the results in Figure 9 in which the truncation artificially introduces additional peaks of comparable intensity to the layer FT peak.

## 5.2 Determination of layer thicknesses in multi-layer structures

Multiple layer structures present a more substantial challenge to the FT approaches in general, so the effectiveness of including the differentiation method in the transformation should be assessed in terms of analyzing such a multi-layer structure. The strategy for including the differentiation method is illustrated using a multiple layer (>5) InAs / AlSb heterostructure grown on GaAs. These structures are used for high speed electronic devices. Reflectivity data from such a multi-layer structure is presented next to assess how well the differentiation process combined - in this case - with the  $Q_z^4$  multiplication can extract important layer thickness information.

As noted above, Fourier analysis affords a reasonably straightforward method for determining layer thicknesses, though initially it may be difficult to interpret which layer thicknesses are represented by which FT peaks in these more complex, multi-layer structures. One method for identifying FT peaks is to Fourier transform simulated x-ray reflectivity scans of the structure adding one layer at a time. By tracking the changes to FT peaks with the addition of layers, it is possible to identify the relationship between the FT peaks and the particular layer thicknesses. This process was carried out for the AlSb/InAs structure that is illustrated in Figure 15.

InAs 20 Å	<b>contact cap</b>
In <sub>0.4</sub> Al <sub>0.6</sub> As 40 Å	<b>hole layer</b>
AlSb 12 Å	<b>electron barrier</b>
<i>n</i> -type InAs 12 Å	<b>donor layer</b>
AlSb 75 Å	<b>electron barrier</b>
InAs 150 Å	<b>channel 2DEG</b>
AlSb 500 Å	<b>electron barrier</b>
Al <sub>0.7</sub> Ga <sub>0.3</sub> Sb 0.3 μm	<b>buffer</b>
AlSb 2.0 μm	<b>buffer</b>
SI GaAs	<b>substrate</b>

Fig. 15. Schematic of InAs / AlSb multi-layer structure

Starting with the lower AlSb electron barrier, this process is shown in Figure 16 through Figure 22.

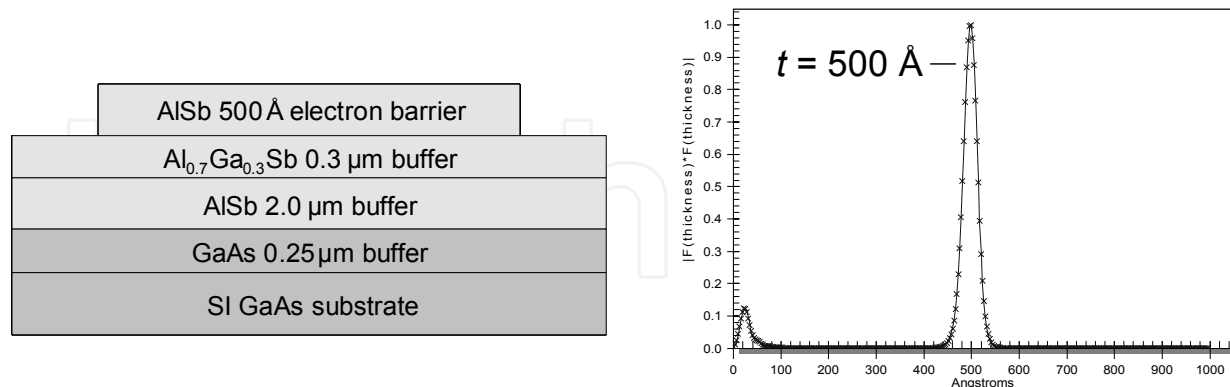


Fig. 16. Simulated reflectivity scan FT of the structure up to the lower AlSb electron barrier

Figure 16 shows the Fourier transform of the reflectivity data; peaks for the buffer layers are not present (beyond the scale of the graph in Figure 16) which indicates that the buffer layers are too thick to yield measurable thickness fringes in the reflectivity scan and therefore do not yield FT peaks. In effect, the fringe spacing for these thick layers is very small ( $\sim 8$  arcsec for a  $2.0 \mu\text{m}$  thick AlSb layer on GaAs using  $\text{Cu } \alpha_1$  radiation) and is readily washed out with even small magnitude beam divergence or curvature that would be typical for modern x-ray sources, equipment, and substrates. The lower AlSb electron barrier, on the other hand, yields a FT peak corresponding to its thickness ( $500 \text{ \AA}$ ). As shown in Figure 17, addition of the InAs electron channel to the simulation yields a new peak at the channel thickness ( $150 \text{ \AA}$ ), and shifts the original lower AlSb barrier FT peak by approximately the channel thickness. The peak labeled  $t_2$  in Figure 17 thus represents the sum of those two layer thicknesses.

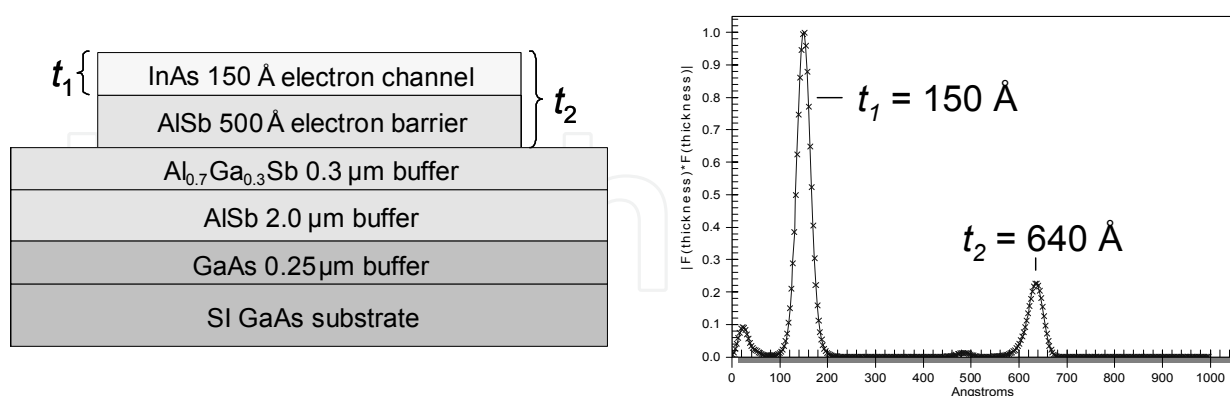


Fig. 17. Simulated reflectivity scan FT of the structure up to the InAs channel

Next, as shown in Figure 18, adding the  $75 \text{ \AA}$  AlSb electron barrier and doped  $12 \text{ \AA}$  InAs layer to the simulation introduces a new FT peak ( $t_1$ ) representing the sum of the two new layers. The InAs channel peak, which is now  $t_2$  in Figure 18, is still present but is very weak. Peak  $t_3$  represents the sum of the InAs channel, middle AlSb barrier, and doped InAs layer thicknesses. FT peak  $t_4$  in Figure 18 represents the sum of the four layer thicknesses above the buffer layers.

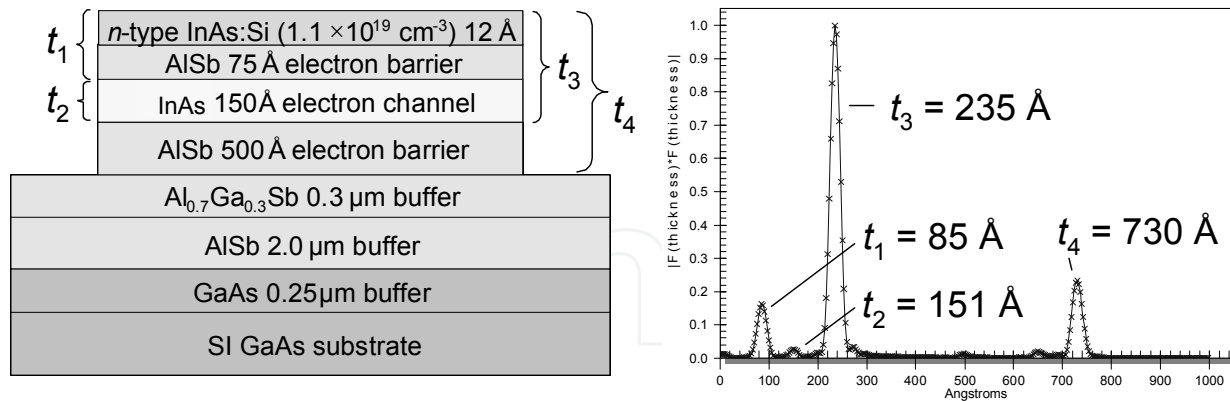


Fig. 18. FT of simulated reflectivity scan of the structure up to the middle AISb electron barrier. Adding the upper 12 Å AISb electron barrier, we see in Figure 19 a shift of peaks  $t_1$ ,  $t_3$ , and  $t_4$ , by approximately the thickness of the new layer.

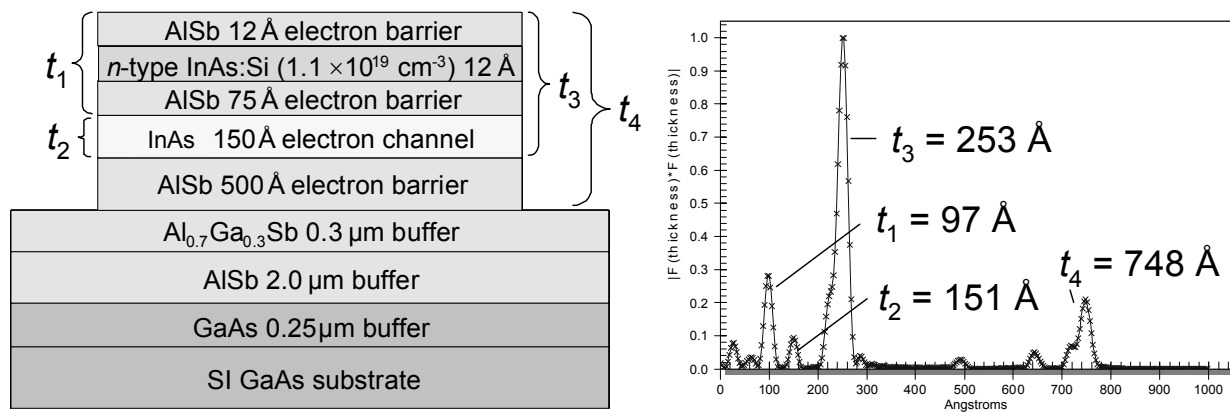


Fig. 19. FT from simulated reflectivity scan of the structure up to the top AISb electron barrier

Carrying this process through to the top of the structure in Figure 20 and 21, we arrive at the relationships between the FT peaks and layer thicknesses summarized in Figure 22.

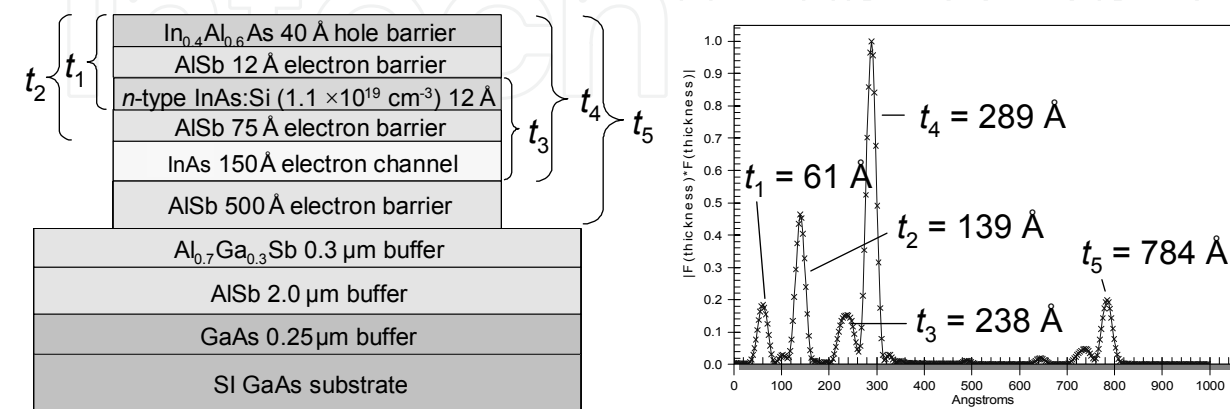


Fig. 20. FT of simulated reflectivity scan of the multi-layer structure up to the InAlAs hole barrier

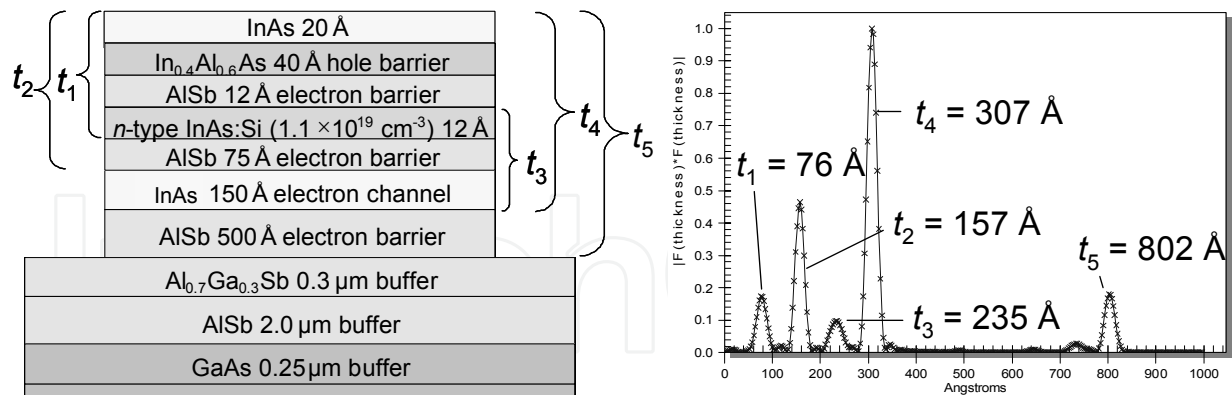


Fig. 21. FT of simulated reflectivity scan of the structure up to the InAs cap layer

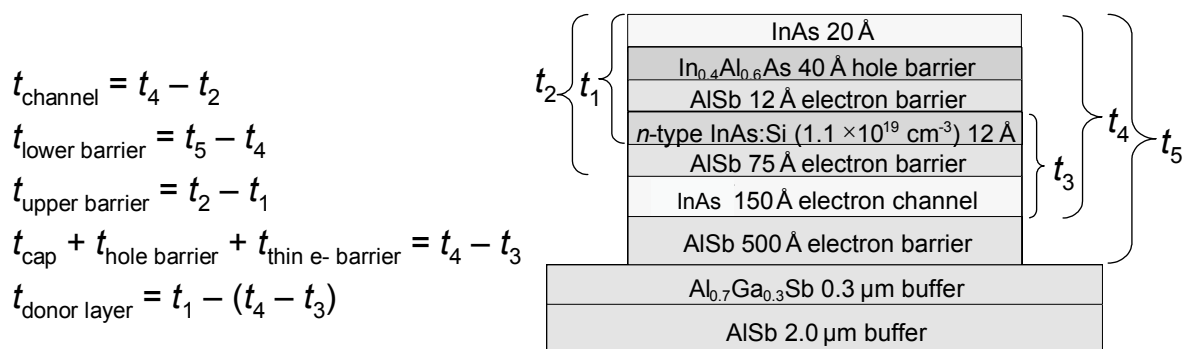


Fig. 22. Relationships between various layer thicknesses and the XRR FT peaks

Through a series of simulated reflectivity scans and the application of the  $Q_z^4$  multiplication and the differentiation described above to the simulation scans, four clear peaks are expected to emerge from the FT. These peaks represent different combinations of the layer thicknesses as identified in Fig. 23. For example, layer “ $t_1$ ” is a combination of the thicknesses of the top four layers,  $t_2$  is a combination of the top five layers,  $t_3$  is from the bottom three layers and  $t_4$  is a sum of thicknesses from the entire stack. Figure 24 shows the experimental specular reflectivity scan from this structure, and the FT of the data after multiplication by  $Q_z^4$  and differentiation as described above for the AlN layer. A simulation based on the FT values is included with the experimental reflectivity data as a dashed line. The FT transform of the processed data clearly show the same four peaks. With these values, the thicknesses of several of the individual layer peaks can be determined. Of prime importance is the thickness of the InAs channel layer. This is  $t_4 - t_2 = 150 \text{ \AA}$  which is the intended thickness and matches that from the best fit XRR simulation ( $154 \text{ \AA}$ ) as well as transmission electron microscopy measurements ( $148\text{-}152 \text{ \AA}$ ). The other layer thicknesses obtained by our new method also match those from the simulated reflectivity scan and from TEM. In fact, even the thin InAs donor layer (This can be obtained, for example, as  $t_1 + t_3 - t_4$ ) is extracted. Using the values in the transformation, the layer thickness is  $10 \pm 3 \text{ \AA}$ , also comparable to the simulated value ( $10 \text{ \AA}$ ) and the TEM measurement ( $10 \pm 3 \text{ \AA}$ ). The benefit with the differentiation approach is that the pulse truncation peak near the origin would overwhelm the peaks due to the thinner layers using any of the previously published processes. The identification of these peaks is confirmed by FT transforms of simulated

scans which also shows that errors related to ignoring refractive index differences from layer to layer are small (thickness differences of less than  $\pm 2 \text{ \AA}$ ).

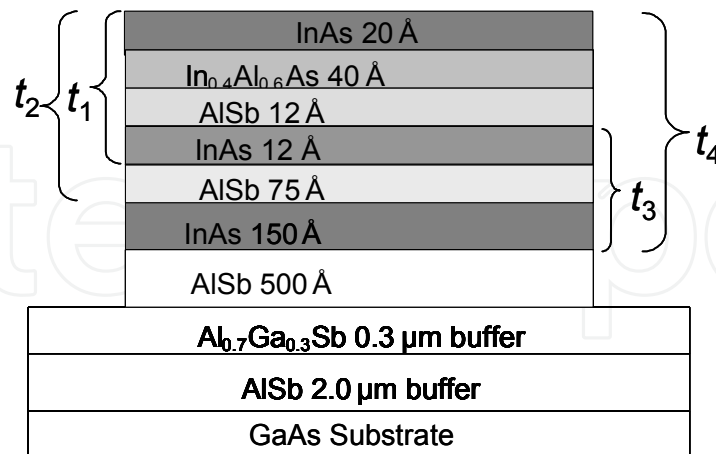


Fig. 23. Schematic of AlSb / InAs heterostructures.  $t_1$ ,  $t_2$ ,  $t_3$ , and  $t_4$  represent the major thickness values from the FT

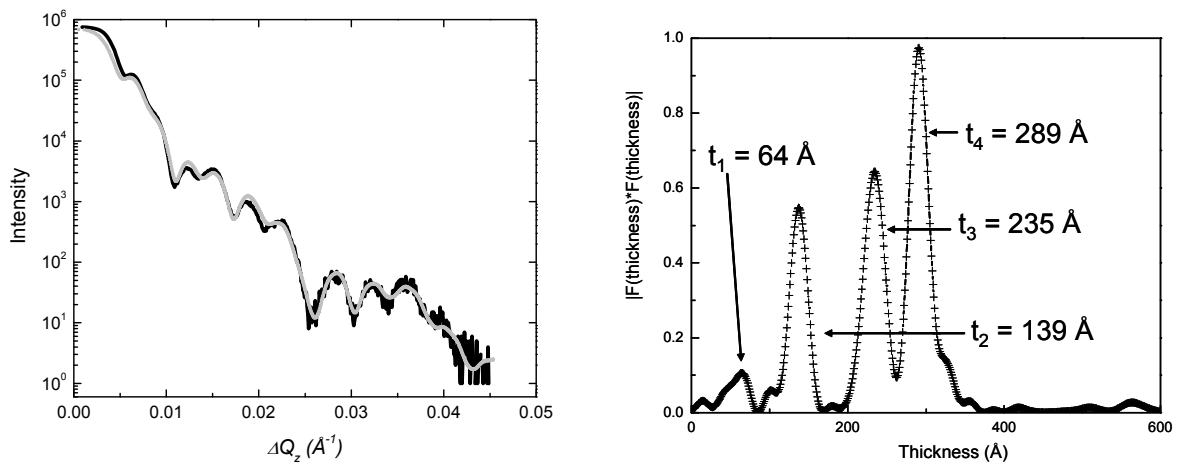


Fig. 24. The specular reflectivity scan and simulation (left, simulation is gray line superimposed on the experimental data, black line) and the FT (right) - after  $Q_z^4$  leveling and differentiation - with the extracted film thicknesses

## 6. Summary

Fourier transforms of X-ray reflectivity scans from multi-layer structures provide useful layer thickness information. A challenge in the transform process is to address the  $Q_z^{-4}$  sloping background which is present with the layer thickness fringe oscillations. Previous studies included several different methods to address this sloping background issue with limited success. Our approach combines one of these previous methods - logarithmic compression or  $Q_z^4$  multiplication - with differentiation of the x-ray reflectivity data. The differentiation more effectively separates the contribution from the sloping background from the thickness fringe oscillations, making the subsequent Fourier transform more

closely related to only the layer thicknesses. This approach is also less susceptible to the presence of a limited number of thickness oscillations or a truncated data set. Data from a single layer (320 Å AlN on an Al<sub>2</sub>O<sub>3</sub> substrate) was utilized to compare the results from each of the previous techniques with the differentiation step. The combination of the differentiation step with either the logarithmic compression or the  $Q_z^4$  leveling produces clear layer thickness peaks after the Fourier transform.

The differentiation approach described here also proved to be very effective at extracting layer thickness information from multi-layer structures that produce complicated specular x-ray reflectivity scans. The Fourier transform produces a series of sharp peaks that originate from different layer thicknesses. The peaks represent the combination of different layer thicknesses and the thickness of each layer can be determined with the assistance of the use of specular x-ray reflectivity simulation scans. This process was demonstrated for an InAs / AlSb multi-layer structure. This technique has applications to any multi-layer system with thin layers including complex optical coatings, multi-layer metallic coatings for giant magnetoresistance measurements and for any other multi-layer structure that can be measured using specular x-ray reflectivity scans.

## 7. Acknowledgments

The authors acknowledge funding for this work from the National Science Foundation and Northrop Grumman, Inc.

## 8. References

- Banerjee, S., G. Raghavan, et al. (1999). *Journal of Applied Physics* 85: 7135.
- Bowen, D. K. and B. K. Tanner (1998). *High Resolution X-ray Diffractometry and Topography*. Bristol, PA, Taylor & Francis Inc.
- Daillant, J. and A. Gibaud (1999). *X-ray and Neutron Reflectivity: Principles and Applications*. Berlin, Heidelberg, Springer Verlag.
- Durand, O. (2004). *Thin Solid Films* 450: 51-59.
- Li, M., M. O. Muller, et al. (1996). *Journal of Applied Physics* 80: 2788.
- Parratt, L. G. (1954). *Physical Review* 95: 359-369.
- Peralta, L. G. d. and H. Temkin (2003). *Journal of Applied Physics* 93(4): 1974-1977.
- Russel, T. P. (1990). *Mater. Sci. Rep.* 5: 171.
- Sakurai, K. and A. Iida (1992). *Adv. X-ray Anal.* 35: 813.
- Wormington, M., C. Panaccione, et al. (1999). *Philosophical Transactions of the Royal Society of London A* 357: 2827-2848.



## **Fourier Transforms - Approach to Scientific Principles**

Edited by Prof. Goran Nikolic

ISBN 978-953-307-231-9

Hard cover, 468 pages

**Publisher** InTech

**Published online** 11, April, 2011

**Published in print edition** April, 2011

This book aims to provide information about Fourier transform to those needing to use infrared spectroscopy, by explaining the fundamental aspects of the Fourier transform, and techniques for analyzing infrared data obtained for a wide number of materials. It summarizes the theory, instrumentation, methodology, techniques and application of FTIR spectroscopy, and improves the performance and quality of FTIR spectrophotometers.

### **How to reference**

In order to correctly reference this scholarly work, feel free to copy and paste the following:

Benjamin Poust and Mark Goorsky (2011). Enhanced Fourier Transforms for X-Ray Scattering Applications, Fourier Transforms - Approach to Scientific Principles, Prof. Goran Nikolic (Ed.), ISBN: 978-953-307-231-9, InTech, Available from: <http://www.intechopen.com/books/fourier-transforms-approach-to-scientific-principles/enhanced-fourier-transforms-for-x-ray-scattering-applications>

**INTECH**  
open science | open minds

### **InTech Europe**

University Campus STeP Ri  
Slavka Krautzeka 83/A  
51000 Rijeka, Croatia  
Phone: +385 (51) 770 447  
Fax: +385 (51) 686 166  
[www.intechopen.com](http://www.intechopen.com)

### **InTech China**

Unit 405, Office Block, Hotel Equatorial Shanghai  
No.65, Yan An Road (West), Shanghai, 200040, China  
中国上海市延安西路65号上海国际贵都大饭店办公楼405单元  
Phone: +86-21-62489820  
Fax: +86-21-62489821

© 2011 The Author(s). Licensee IntechOpen. This chapter is distributed under the terms of the [Creative Commons Attribution-NonCommercial-ShareAlike-3.0 License](#), which permits use, distribution and reproduction for non-commercial purposes, provided the original is properly cited and derivative works building on this content are distributed under the same license.

IntechOpen

IntechOpen